FOI
SWEDISH DEFENCE
RESEARCH AGENCY

FOI-R--0136--SE
June 2001
ISSN 1650-1942
Scientific report

Robin Olsson

Engineering method for prediction of impact response and damage in sandwich panels

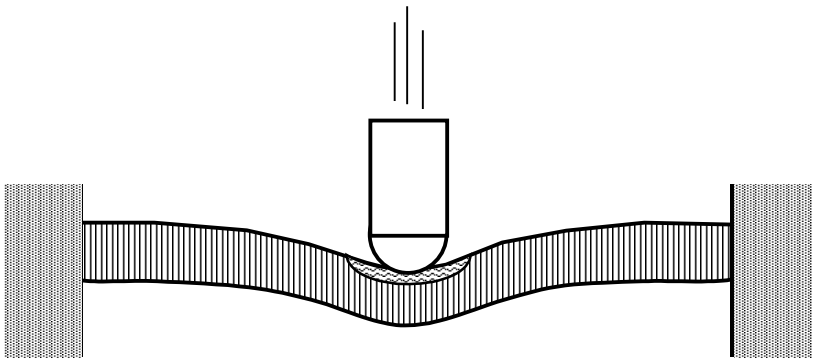

Aeronautics Division, FFA
SE-172 90 Stockholm
Sweden

SWEDISH DEFENCE RESEARCH AGENCY

Aeronautics Division, FFA
SE-172 90 Stockholm
Sweden

FOI-R--0136--SE

June 2001

ISSN 1650-1942

Scientific report

Robin Olsson

Engineering method for prediction of impact response and damage in sandwich panels

Issuing organization	Report number, ISRN	Report type
FOI – Swedish Defence Research Agency Aeronautics Division, FFA SE-172 90 Stockholm Sweden	FOI-R--0136--SE	Scientific report
	Research area code 7. Vehicles	
	Month year June 2001	**Project no.** E824469
	Customers code 5. Contracted Research	
	Sub area code 72. Aeronautical Systems	

Author/s (editor/s)	Project manager
Robin Olsson	Robin Olsson
	Approved by Magnus Linde, Acting head of Aeronautics Division
	Scientifically and technically responsible Sören Nilsson

Report title

Engineering Method for Prediction of Impact Response and Damage in Sandwich Panels

Abstract (not more than 200 words)

An engineering method is suggested for prediction of impact response and damage of flat sandwich panels. The approach accounts for local core crushing, delamination and large face sheet deflections and does not rely on empirical indentation laws. Different models are suggested depending upon the impactor mass being either larger or significantly smaller than the mass of the impacted panel. The solution for large mass impact is based on closed form expressions. The solution for small mass impact is obtained from a dimensionless two-parameter integral equation. The validity of the approach is demonstrated on a number of static indentation experiments and impacts on sandwich panels.

Keywords

Composite materials, Impact, Impact damage, Impact loads, Indentation, Sandwich structures

Further bibliographic information	Language English

To appear in *Journal of Sandwich Structures and Materials*

ISSN 1650-1942	Pages 48 p.
	Price acc. to pricelist **Security classification: Open**

Utgivare	Rapportnummer, ISRN	Klassificering
Totalförsvarets Forskningsinstitut - FOI	FOI-R--0136--SE	Vetenskaplig rapport
Avdelningen för flygteknik, FFA	**Forskningsområde**	
172 90 Stockholm	7. Bemannade och obemannade farkoster	
	Månad, år	**Projektnummer**
	Juni 2001	E824469
	Verksamhetsgren	
	5. Uppdragsfinansierad verksamhet	
	Delområde	
	72. Flygsystem	
Författare/redaktör	**Projektledare**	
Robin Olsson	Robin Olsson	
	Godkänd av	
	Magnus Linde, Stf. avdelningschef, Flygteknik	
	Tekniskt och/eller vetenskapligt ansvarig	
	Sören Nilsson	

Rapportens titel (i översättning)

Ingenjörsmässig metod för förutsägelse av slagrespons och slagskador i dubbelskalspaneler

Sammanfattning (högst 200 ord)

En ingenjörsmässigmässig metod föreslås för att förutsäga slagrespons och slagskador hos plana dubbelskalspaneler. Metoden tar hänsyn till lokal krossning av kärnmaterialet, delaminering och stora utböjningar av täckskiktet samt är oberoende av empiriska intryckningssamband. Olika modeller föreslås beroende på om slagkroppens massa är större eller väsentligt mindre än massan hos den slagna panelen. Lösningen för slag med stora massor baseras på uttryck på sluten form. Lösningen för slag med små massor erhålls från en dimensionslös integralekvation med två parametrar. Metodens giltighet demonstreras på ett antal statiska intryckningsprov samt på slag mot dubbelskalspaneler.

Nyckelord

Kompositmaterial, slag, slagskador, slagbelastning, intryckning, dubbelskalspaneler

Övriga bibliografiska uppgifter	Språk Engelska

Godkänd för publicering i *Journal of Sandwich Structures and Materials*

ISSN 1650-1942	**Antal sidor:** 48 s.
Distribution enligt missiv	**Pris: Enligt prislista** **Sekretess: Öppen**

Contents

1. Introduction

Polymer composite laminates find increasing use in structures where weight is a major consideration, e.g. aircraft and high speed boats and trains. Sandwich structures with laminated face sheets offer additional improvements in bending stiffness per unit weight and may reduce the number of parts in manufacturing. However, the use of composite laminates is hampered by their poor resistance to formation of impact damage, which may severely reduce the structural strength and stability [1-2]. Similar effects have been observed for sandwich panels [3-7]. For this reason extensive research has been dedicated to the problem of impact on composite laminates [1-2] while the work on sandwich structures is somewhat more limited [3]. An efficient approach to analyze the effect of impact on structures is to separately address *impact damage resistance*, which deals with the response and damage caused by impact, and *impact damage tolerance*, which deals with the effect of the damage on strength and stability of the structure. In the present paper we address impact damage resistance of flat sandwich panels.

The work on impact damage resistance of sandwich panels is dominated by experimental studies quantifying damage and, in some cases, response for a given geometry. Extensive fractographical studies of impact damage can be found in [8-9]. Damage in laminated sandwich face sheets may consist of matrix cracks, delaminations and fiber fracture but are much more local than in monolithic laminates. Delaminations may grow under loading, and matrix cracks and fiber fracture cause stress concentrations which may cause premature skin failure [4]. Impacted sandwich panels also suffer from core crushing, sizeable dents and sometimes core cracking or debonding. The loss of core stiffness due to crushing may cause local skin buckling which is enhanced by the presence of a dent [4, 7].

Indentation and shear deformation of sandwich panels are often of the same order or greater than the bending deformation. Thus, the inclusion of indentation and shear effects is imperative for a successful prediction of impact response and damage. Published analytical models for sandwich panel impact response assume elastic behavior, and are thus unable to predict damage growth. In most cases they have been based on empirical load-indentation models [10-15] while analytical elastic indentation models show poor accuracy [7, 10, 16]. Dynamic FE-simulations with progressive damage modeling have been more successful but are extremely time consuming [17-18]. A recent example focused on core crushing can be found in [19]. Analytical models for the

wave controlled impact response caused by relatively small impactors were given in [20-21]. However, in [21] it was shown that the assumptions in [20] are invalid in most cases of concern in sandwich structures.

The main reason for the poor accuracy of purely elastic indentation models is the neglect of core crushing and large face sheet deflections. These effects were incorporated in an analytical indentation model based on large deflection plate theory and membrane theory for a face sheet on an elastic-ideally plastic core [22]. A similar model limited to membrane theory and an ideally plastic core was presented some years later [23]. The elastic-plastic core description was recently used in a static FE-analysis, which combined a local indentation model with a global deflection model [24].

The aim of the present paper is to propose an engineering method to predict impact response and damage formation in sandwich panels by use of simple, yet sufficiently accurate models. The predictions may be used in preliminary design for improving impact tolerance or for damage estimation in damage tolerance analysis. Furthermore, they allow screening for critical cases among a large number of impact threats. It is assumed that the impact damage is local enough to neglect its influence on the global panel behavior, which allows a local model for the damage area. Firstly, the local model for indentation and damage formation is described. Then, criteria for initiation and growth of face sheet and core damage are derived. Subsequently, the response types associated with flexural/shear wave propagation and with global deflection are described and governing criteria formulated. Finally, appropriate structural models for each response type are suggested and applied to published experiments.

2 Effective properties of orthotropic panels

For orthotropic plates we define an effective plate stiffness D^* [21] and shear stiffness S^*

$$D^* \approx \sqrt{D_{11}D_{22}(\eta+1)/2} \qquad \text{where } \eta = (D_{12}+2D_{66})/\sqrt{D_{11}D_{22}} \tag{1}$$

$$S^* = \sqrt{A_{44}^* A_{55}^*} = \sqrt{K_{44}A_{44}K_{55}A_{55}} \tag{2}$$

where K_{ij} are the shear factors and D_{ij} and A_{ij} are the bending and shear stiffness components given by laminated plate theory [25]. Appendix A gives explicit expressions for the stiffness components of sandwich panels with thin stiff face sheets on a soft core [26]. The indentation theory used in the present paper was derived for axisymmetric cases. However, it has also been successfully applied [27] to orthotropic honeycomb cores and face sheets with (0/±45) and (0/90) lay-ups by use of Eq. (1) and the following average properties:

$$\begin{aligned} &Q_z^* = E_z/\left(1-\nu_{rz}^{*2}\,E_z/E_r^*\right) = E_z/\left(1-\nu_{zr}^{*2}\,E_r^*/E_z\right) \\ &\text{where } \nu_{rz}^* = \sqrt{\nu_{xz}\nu_{yz}} \qquad \text{and } \left[E_r^*,\nu_r^*\right] = \tfrac{1}{2\pi}\int_0^{2\pi}\left[E_r(\theta),\nu_r(\theta)\right]d\theta \end{aligned} \tag{3}$$

Foam cores are usually more or less isotropic but viscoelastic effects are often significant [18, 42]. If the elastic properties of anisotropic cores and faces are incompletely defined the approximation $Q_z \approx E_z$ may often be used, since fiber reinforced face sheets usually satisfy ν_{rz}^*<0.5 and E_z/E_r^* <<1, while honeycomb cores satisfy ν_{zr}^*<0.5 and E_r^*/E_z <<1.

3. Local model for indentation

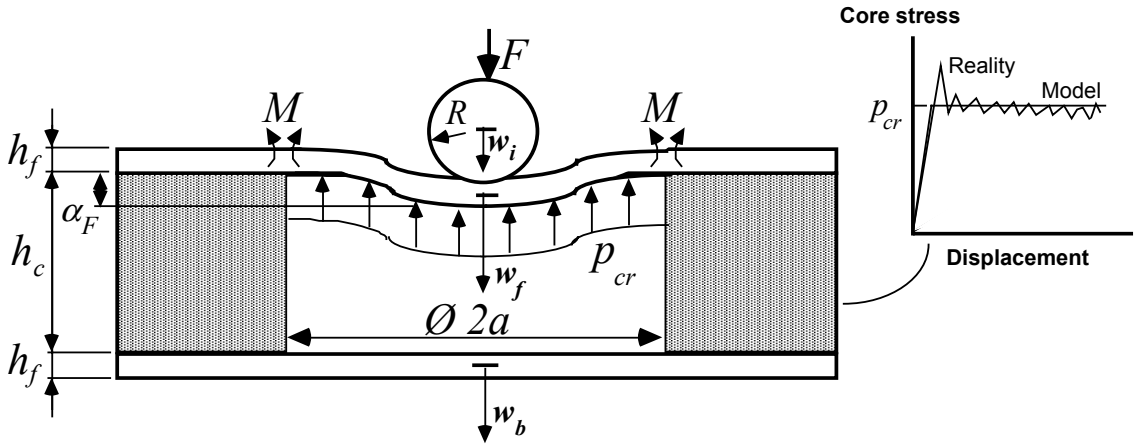

Fig. 1: Indentation model

The indentation α of a sandwich panel may be separated in two parts, Fig. 1. The indentation of the face sheet α_H, is usually of minor importance. The indentation due to local face sheet deflection α_F, is often considerably larger than the face sheet thickness. Thus, α is given by:

$$\alpha = \alpha_H + \alpha_F \quad \text{where} \quad \alpha_H = w_i - w_f \quad \text{and} \quad \alpha_F = w_f - w_b \qquad (4)$$

where w_i is the displacement of the impactor mass center, and w_f and w_b are the mid-plane deflections of the front and back face skins. The present indentation model [22], Fig. 1, considers large deflections due to a contact load on an elastic face sheet with a foundation having an elastic-ideally plastic out-of-plane behavior, where the yield stress represents the out-of-plane crush stress of the core.

Hertzian indentation of the face sheet is assumed, which results in the following relation between the total load F, the face sheet indentation α_H and the contact radius c [22]:

$$\alpha_H = \left(F/k_H\right)^{2/3} \qquad c = \sqrt{R\alpha_H} \qquad \text{where } k_H = \tfrac{4}{3} Q_H \sqrt{R} \qquad (5)$$

where R is the indentor tip radius and the effective out-of-plane stiffness, Q_H, is given by

$$1/Q_H = 1/Q_{zi}^* + 1/Q_{zf}^* \qquad (6)$$

and indices *i* and *f* refer to impactor and face sheet. The elastic region of the core is modeled as a Winkler foundation, i.e. without out-of-plane shear stiffness. Such a core is in a uniaxial stress state with stresses and displacements related through the elastic foundation stiffness k_F:

$$\sigma_z = -k_F \alpha_F \tag{7}$$

The deviation from a uniaxial stress state is small [28] for a core thickness less than:

$$h_{c\max} = h_f \tfrac{32}{27} \left(\tfrac{4}{3} Q_f^* \big/ Q_{zc}^* \right)^{1/3} \quad \text{where} \quad Q_f^* = 12 D_f^* \big/ h_f^3 \tag{8}$$

where D_f^* is the effective plate stiffness of the face sheet. The foundation stiffness in thick cores is not uniquely defined since displacements and stresses cannot simultaneously be matched to the proper three-dimensional solution [29]. The available solution for isotropic cores may also be applied for honeycombs, since they have a similar relation between the average out-of-plane shear modulus and Young's modulus. The following foundation stiffness matches deflections well for thick cores and matches stresses and deflections for thin cores:

$$\begin{aligned} & k_F = Q_{zc}^* \big/ h_c^* \quad \text{where } h_c^* = \begin{cases} h_c / 1.38 & \text{for } h_c \le h_{c\max} \\ 2 h_{c\max} & \text{for } h_c > h_{c\max} \end{cases} \\ & \left(\text{stress matched:} \qquad h_c^* = \left(\tfrac{27}{64} \right)^2 2 h_{c\max} \qquad \text{for } h_c > h_{c\max} \right) \end{aligned} \tag{9}$$

Local deflection prior to core crushing at the critical crush load F_{cr} is modeled using small deflection theory for a plate on an elastic foundation, which is given by [22]:

$$\alpha_F = \tfrac{1}{8} F \Big/ \sqrt{k_F D_f^*} \qquad \text{for} \qquad F \le F_{cr} \tag{10}$$

Local deflection after crushing is modeled using small or large deflection plate theory (subscript *p*) or membrane theory (subscript *m*) for a face sheet on an outer elastic region and an inner region with a uniform reactive pressure. The solution is simplified by introducing dimensionless load $\overline{F}_i$, and moment $\overline{M}$ and radius $\overline{a}_i$ at the edge of the crushed region:

$$\overline{F}_i = F_i \sqrt{k_F / D_f^*} \Big/ (\pi p_{cr}) \quad \overline{M} = (M / p_{cr}) \sqrt{k_F / D_f^*} \quad \overline{a}_i = \sqrt{\pi p_{cr} a_i^2 / F_i} \tag{11}$$

where $i = p$ or m and p_{cr} is the crush stress of the core. The parameter $\bar{a}_i^2$ quantifies the load fraction carried by core crushing. The dimensionless moment $\overline{M}$ and crush radii $\bar{a}_p$ and $\bar{a}_m$ for the plate and membrane solutions as functions of the load $\bar{F}_i$ are shown in Fig. 2 and were tabulated in [27].

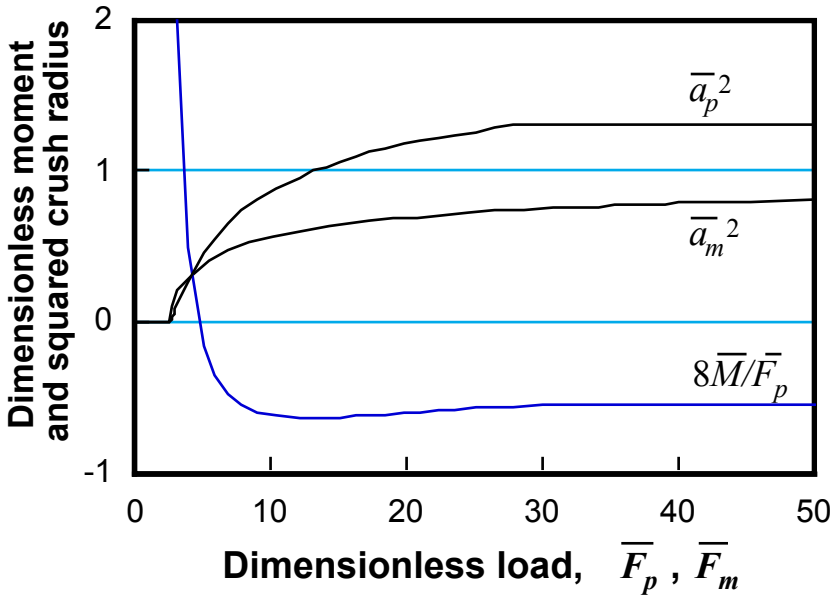

Fig. 2: Dimensionless indentation crush radius and edge moment

The small deflection plate solution after core crushing is given by [22]:

$$\alpha_F = \alpha_{cr} + \frac{F_p^2 \bar{a}_p^2}{16\pi^2 p_{cr} D_f^* \left(1+\nu_r^*\right)}\left[\left(3+\nu_r^*\right) - \bar{a}_p^2\left(5+\nu_r^*\right)/4 + 8\overline{M}/\overline{F}_p\right]$$
$$\text{for } F_{cr} < F_p < F_{dth} \quad \text{where } \alpha_{cr} = \alpha_F\left(F_{cr}\right) \tag{12}$$

where F_{dth} is the delamination threshold load and F_p is the load according to small deflection theory. Prior to delamination the total load F at a given deflection $\alpha_F(F_p)$ is obtained by multiplying F_p with the following magnification factor, which considers the additional load carried by large deflection membrane effects [22]:

$$F/F_p = \sqrt{\left(1+\bar{k}_m \bar{\alpha}_\Delta^2\right)/\left[1+\left(\bar{k}_m - \bar{k}_{mcl}\right)\bar{\alpha}_\Delta^2\right]^\mu}$$
$$\text{where } \bar{\alpha}_\Delta = \left(\alpha_F - \alpha_{cr}\right)/h_f \tag{13}$$

and the dimensionless membrane stiffnesses k_m, k_{mcl} and the exponent μ [22] are shown in Fig. 3.

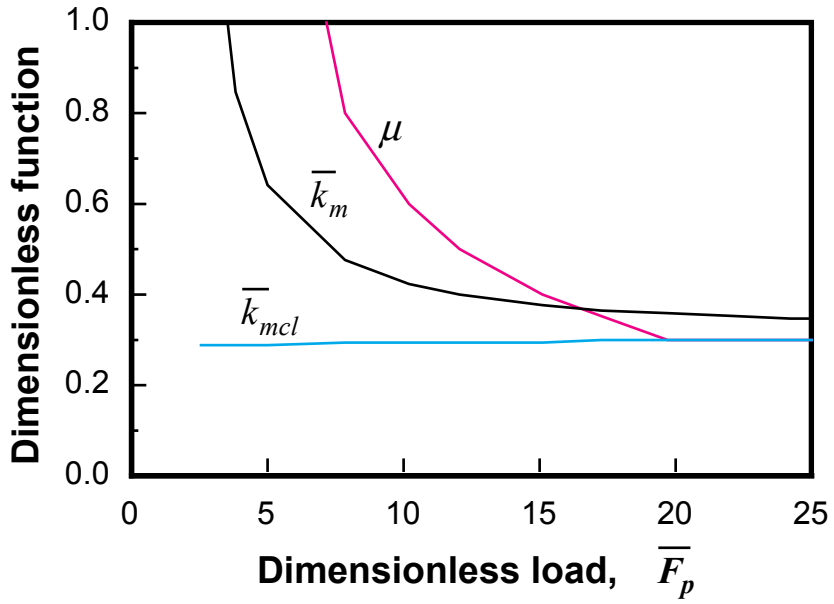

Fig. 3: Functions for large deflection plate indentation model

Delaminations severely reduce the bending stiffness but not the membrane stiffness. Thus, the behavior after delamination is essentially given by the membrane solution, which also is a good approximation for undamaged face sheets when deflections exceed four face sheet thicknesses, which is common for thin metal skins. As shown in Appendix C the membrane solution in [22] is modified to the following form in case of a finite contact radius:

$$\alpha_F = \alpha_{cr} + \left[1 + Cs_1 - (1+C)s_1^2\right] w_m + \tfrac{1}{2} s_1^2 \, a_m^2 / R \qquad \text{for } F_{dth} \le F_m < F_f$$

$$\text{where } w_m = f_w \left[\frac{F_m^2 \overline{a}_m^2}{2 p_{cr} E_{rf}^* h_f} \right]^{1/3} \tag{14}$$

and w_m is the solution for a concentrated load F_m [22]. Here F_f is the load at fiber fracture, f_w is a function close to unity and s_1 is a small parameter expressing the contact radius as fraction of the crush radius. The functions f_w and C+2 [22] are shown in Fig. 4.

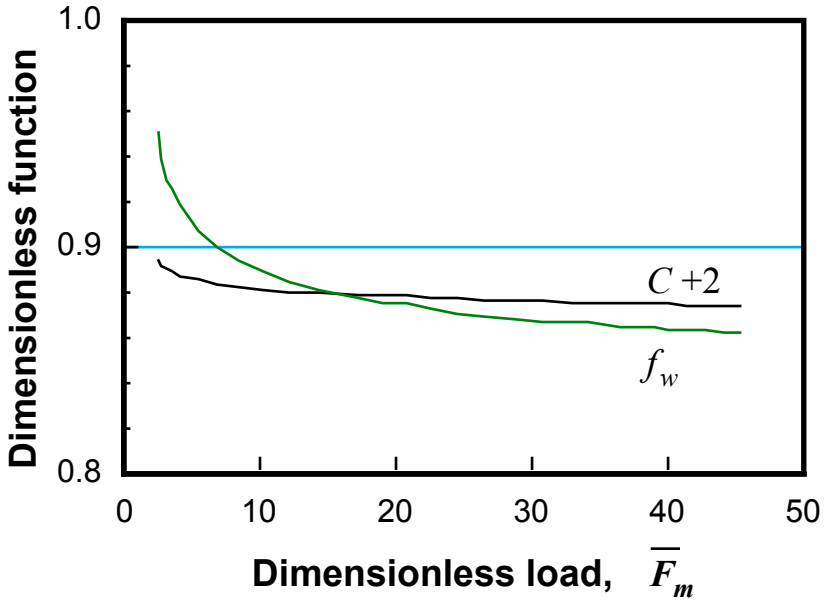

Fig. 4: Functions for membrane indentation model

The normalized contact radius s_1, derived in Appendix C, is given by

$$s_1 = r_1/a_m = -C/\left[a_m^2/(w_m R) - 2(1+C)\right] \tag{15}$$

The membrane contact radius r_1 is illustrated in Fig. 5.

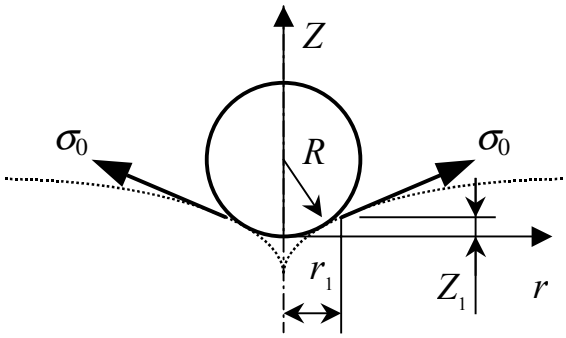

Fig. 5: Deformation of membrane over spherical impactor

The number of delaminations quickly increases to a saturated number, n_{max} [30]. The total load F after delamination initiation may then be separated into the contribution due to membrane forces F_m and the critical out-of-plane shear load F_d (derived in Appendix B) for propagation on n_{max} delaminations:

$$F = F_m + F_d(n_{\max}) = F_m + \pi\sqrt{32 D_f^* G_{IIc} \Big/ \left[(n_{\max}+2)\left(1-\bar{a}_m^2/2\right)\right]} \qquad (16)$$

where it is assumed that the face sheet is completely delaminated ($\bar{a}_d = \bar{a}_m$) in the crush region. The predicted load-indentation relation can usually be approximated by a power-law:

$$F \approx k_\alpha \alpha^q \qquad (17)$$

Hertzian indentation (q=3/2) dominates at low loads and for thick faces and stiff cores. For most cases of interest in sandwich structures the Hertzian indentation is negligible and the combined action of softening due to core crushing and stiffening due to face sheet membrane effects results in a more or less linear load-indentation relation (q≈1). Note that the suggested solution only is applicable prior to fiber fracture and penetration.

4. Criteria for damage growth

The critical load for core crushing F_{cr} is obtained by combination of Eqs (7) to (10):

$$\begin{aligned} F_{cr} &= 8 p_U \sqrt{D_f^* h_c \big/ \left(1.38 Q_{zc}^*\right)} \qquad \text{for} \quad h_c \le h_{c\max} \\ F_{cr} &= 3\sqrt{3}\, p_U \left(2 D_f^* \big/ Q_{zc}^*\right)^{2/3} \qquad \text{for} \quad h_c > h_{c\max} \end{aligned} \tag{18}$$

where p_U is the compressive strength of the core, Fig. 1, which usually is larger than the crush stress. For thick cores the foundation stiffness for stress matching in Eq. (9) has been applied. The presence of matrix cracks is a necessary prerequisite for delamination. Stresses close to the contact load may deviate significantly from plate theory predictions but stable crack planes will not appear until the stress distribution given by plate theory is recovered. The shear force has a peak close to the contact radius c where the peak shear stress in plate theory is given by

$$\tau_{\max} = \tfrac{3}{2} F_p \big/ (2\pi c h) \tag{19}$$

Combination of Eqs (5) and (19) then yields the following load F_s for mid-plane shear cracks

$$F_s = \tfrac{4}{3} (\pi h \tau_c)^{3/2} \sqrt{R/Q_\alpha} \tag{20}$$

where τ_c is the transverse shear strength. The load for growth of single delaminations in clamped quasi-isotropic laminates without a reactive core pressure was derived in [31], but has been shown to be applicable to other boundary conditions and lay-ups [30]. The derivation in Appendix B results in an identical load F_{dth} for the *initiation* of delamination growth when a supporting core is included:

$$F_{dth} = \pi \sqrt{32\, D_f^* G_{IIc} \big/ 3} \tag{21}$$

The center membrane strain after delamination may be obtained by considering equilibrium for a spherical cap and the membrane solution in [22]. The derivation in Appendix C yields the following peak strain:

$$\varepsilon_0 = (1-\nu)\sigma_0 = \tfrac{1}{2}(1-\nu)\left[1 \big/ \left(s_1^2 \bar{a}_m^2\right) - 1\right] p_{cr} R/h \tag{22}$$

where the quantity s_1 was defined in Eq. (15). Fiber failure occurs when the peak strain reaches the fiber failure strain ε_f of the material. The predicted strain will be of fairly low accuracy since the membrane Ritz solution is based on a two-parameter assumed mode. The core crush radius a is easily obtained from the last relation in Eq. (11), where the squared dimensionless crush radius $\bar{a}_i^2$ is given by $\bar{a}_p^2$ in Fig. 2 prior to delamination and by $\bar{a}_m^2$ after delamination. From Eq. (11) it is easily observed that the quantity $\bar{a}_i^2$ expresses the fraction of the total load carried by core crushing. For simplicity we assume that fiber fracture causes a complete loss of face sheet stiffness. Thus, in displacement control fiber fracture causes a load drop by a factor $1-\bar{a}_m^2$, i.e. by approximately thirty percent. Similarly, in load control the dimensionless crush radius will be unity so that the crush radius increases by a factor $1/\bar{a}_m$.

5. Determination of response regime

An impact initiates elastic waves propagating from the impact point, where material damping and the scattering waves result in a decaying influence of the corresponding waves. For impact times in the order of the transition time for through-the-thickness waves, the response becomes dominated by three-dimensional wave propagation. For longer impact times flexural waves and shear waves govern the response. For times much longer than the time needed by these waves to reach the plate boundaries the lowest vibration mode of the impactor-plate system predominates. It is common to distinguish between high-velocity and low-velocity impact. However, a recent paper demonstrates that impactor versus plate mass ratio governs the response type [32]. Wave controlled (small mass) impact response occurs when the impactor mass is smaller than one fifth of the wave affected plate mass when a major wave first reaches a boundary. For orthotropic plates it is necessary to consider the ratio of flexural wave speeds in order to determine the boundary first hit by a wave, since it may not be the one closest to the impact. Thus, the maximum wave affected mass, M_{pmax}, is given by the smallest elliptical plate area with aspect ratio $r_x/r_y = (D_{11}/D_{22})^{1/4}$ which touches any of the boundaries when centered at the impact. Quasi-static (large mass) impact response occurs for impactor masses larger than twice the plate mass, or less for plates with large aspect ratios. The mass criteria governing response type are illustrated for an orthotropic plate in Fig. 6.

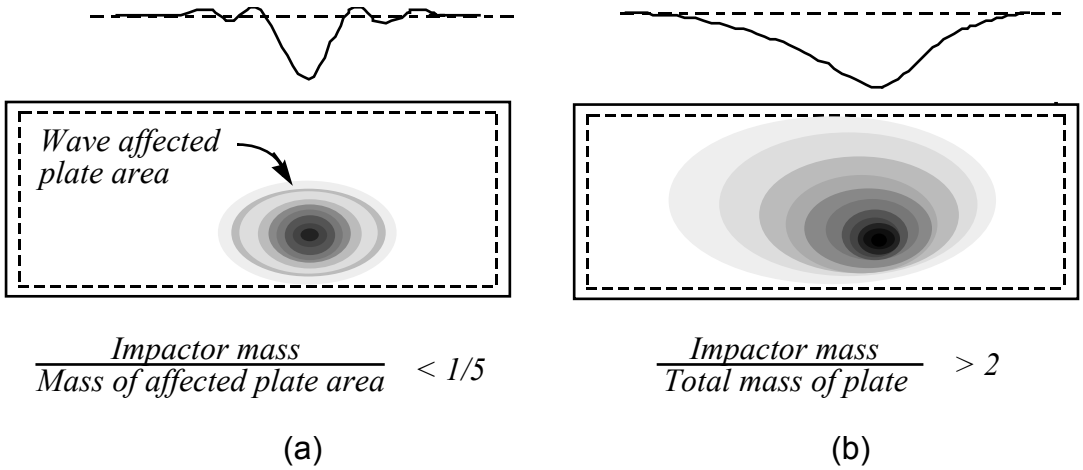

Fig. 6: Mass criteria and panel deflection shapes for small (a) and large (b) mass impact

6. Model for small mass impact response

A solution for small mass impact on sandwich plates was suggested in [20], where the local face sheet deflection was neglected. Evidently, such an assumption is only valid for very small impact loads, and it has been shown [21] that the serial solution suggested in [20] diverges for most cases of concern in conventional sandwich structures. Solutions for monolithic orthotropic plates without shear deformations may be obtained from the isotropic solution by using an effective orthotropic bending stiffness, given in [33] and the appendix of [34]. The definition of D^* in Eq. (1) deviates by less than 2 % from the exact expression for $0 \le \eta \le 10$. However, the low shear stiffness of sandwich panels necessitates the inclusion of shear deformations. The present solution [21] generalizes the solution for transversely isotropic (quasi-isotropic) plates in [35], by use of the effective plate bending stiffness D^* and shear stiffness S^*. Combination of Eq. (1) with the dynamic equations for shear deformable plates results in an integral equation [35], which can be put in the following dimensionless form:

$$\bar{\alpha} = \bar{t} - \int_{\bar{t}_0}^{\bar{t}} \bar{F}(\bar{\tau})\left[(\bar{t}-\bar{\tau}) + \lambda\frac{2}{\pi}\left\{\arctan\left[(\bar{t}-\bar{\tau})/\beta\right] + 2\beta/(\bar{t}-\bar{\tau})\right\}\right] d\bar{\tau} \qquad (23)$$

where the dimensionless force, time and indentation [21, 34] are defined by

$$\bar{F}(\bar{t}) = \bar{\alpha}^q(\bar{t}) \quad \text{where } \bar{t} = t/T \text{ and } \bar{\alpha} = \alpha/(TV_0) \text{ such that } \dot{\bar{\alpha}}(0) = 1 \qquad (24)$$

and the time constant T for an impactor with mass M and velocity V_0 [21, 34] is given by

$$T = \sqrt{M/k_\alpha} \text{ for } q = 1 \quad \text{and} \quad T = \left[M/\left(k_\alpha\sqrt{V_0}\right)\right]^{2/5} \text{ for } q = 3/2 \qquad (25)$$

The dimensionless flexural mobility λ and shear mobility β of the plate [21, 35] are defined by

$$\lambda = M\Big/\left(8T\sqrt{mD^*}\right) \qquad \beta = \sqrt{mD^*}\Big/\left(S^*T\right) \qquad (26)$$

where m is the plate mass per unit area. The small time parameter $\bar{t}_0$ accounts for the action of surface loads over a finite area. We use the definition in [34], originally derived by Sneddon [36] when analyzing forced motion of large plates under a load uniformly distributed within a

radius much smaller than that of the deflected area. For indentation dominated by face sheet deflection (q≈1) we assume that surface loads are applied within the core crush radius, a_i, given by Eq. (11). For Hertzian indentation (q=3/2) we assume that the surface loads are applied within the Hertzian contact radius. For these cases the parameter $\bar{t}_0$ [21] is given by:

$$\begin{aligned} q=1: &\qquad \bar{t}_0 = a^2\sqrt{m/D^*}\,\big/T \approx \tfrac{1}{4\pi}\bar{\alpha}\,k_\alpha V_0\sqrt{m/D^*}\,\big/p_{cr} = k_{tF}\bar{\alpha} \\ q=3/2: &\qquad \bar{t}_0 = c^2\sqrt{m/D^*}\,\big/T = \tfrac{1}{4}\bar{\alpha}RV_0\sqrt{m/D^*} = k_{tH}\bar{\alpha} \end{aligned} \tag{27}$$

Note that $\bar{t}_0$ is a function of the load, in contrast to the assumed constant value used in [33, 35]. Expressions for the flexural moment in Mindlin plates are given on integral form in [35] and on closed form for Kirchhoff plates in [34]. Discretisation and piecewise integration of Eq. (23), using the method suggested in [37], allows the following stepwise determination of the indentation:

$$\begin{aligned} &\bar{\alpha}_0 = 0 \\ &\bar{\alpha}_{N+1} = (N+1)\Delta\bar{t} - \tfrac{1}{2}\Delta\bar{t}^{\,2}\sum_{i=0}^{N}\bar{\alpha}_i^{\,q}(2N-2i+1) \\ &-\lambda\tfrac{2}{\pi}\sum_{i=0}^{N}\bar{\alpha}_i^{\,q}\Big[\Delta\bar{t}(N-i+1)\arctan\Big\{\tfrac{N-i+1}{\beta}\Delta\bar{t}\Big\} - \Delta\bar{t}(N-i)\arctan\Big\{\tfrac{N-i}{\beta}\Delta\bar{t}\Big\} \\ &-\tfrac{1}{2}\beta\ln\Big\{\tfrac{\beta^2+(N-i+1)^2\Delta\bar{t}^{\,2}}{\beta^2+(N-i)^2\Delta\bar{t}^{\,2}}\Big\} + 2\beta\ln\Big\{\tfrac{(N-i+1)\Delta\bar{t}+\bar{t}_0}{(N-i)\Delta\bar{t}+\bar{t}_0}\Big\}\Big] \end{aligned} \tag{28}$$

Following [34] we redefine the dimensionless plate center deflection in [35] as follows:

$$\bar{w}_0 = w_0 8\sqrt{mD^*}\,\big/(MV_0) = \tfrac{2}{\pi}\int_{\bar{t}_0}^{\bar{t}}\bar{F}(\bar{\tau})\{\arctan[(\bar{t}-\bar{\tau})/\beta] + 2\beta/(\bar{t}-\bar{\tau})\}\,d\bar{\tau} \tag{29}$$

which is obtained by dividing the last sum in Eq. (28) with λ. For Kirchhoff plates, β=0, the model in Fig. 7a applies and we may write Eq. (23) as a differential equation [34]:

$$\ddot{\bar{\alpha}} + \lambda q\bar{\alpha}^{q-1}\dot{\bar{\alpha}} + \bar{\alpha}^q = 0 \qquad \bar{\alpha}(0) = 0 \qquad \dot{\bar{\alpha}}(0) = 1 \tag{30}$$

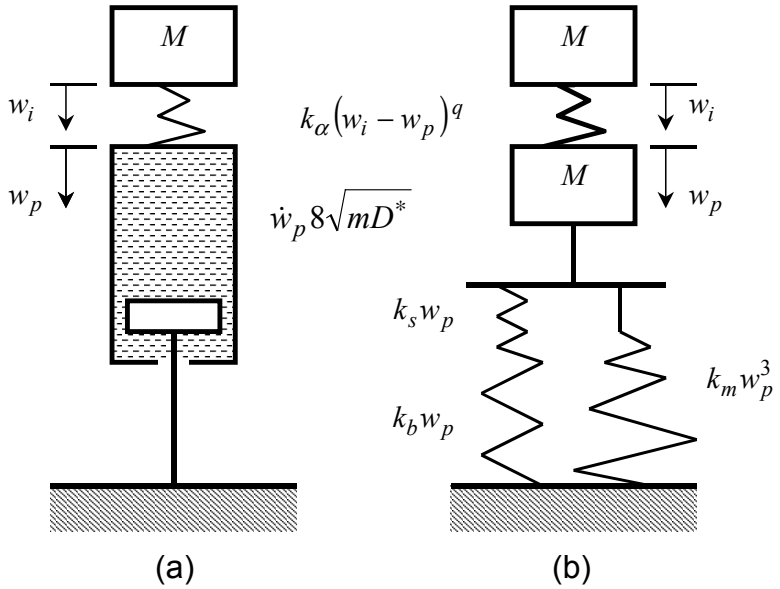

Fig. 7: Response models for small (a) and large (b) mass impact

Closed solutions for sandwich panels (q=1) without shear deformation were given in [21]:

$$\begin{aligned}
&\lambda < 2 \quad \overline{F} = \overline{\alpha} = \sin\left(\bar{t}\sqrt{1-\lambda^2/4}\right)e^{-\lambda\bar{t}/2} \Big/ \sqrt{1-\lambda^2/4} \\
&\lambda = 2 \quad \overline{F} = \overline{\alpha} = \bar{t}e^{-\bar{t}} \\
&\lambda > 2 \quad \overline{F} = \overline{\alpha} = \sinh\left(\bar{t}\sqrt{\lambda^2/4-1}\right)e^{-\lambda\bar{t}/2} \Big/ \sqrt{\lambda^2/4-1} \\
&\overline{w}_0 = \bar{I} = \int_0^{\bar{t}} \overline{F}(\bar{\tau})d\bar{\tau}
\end{aligned} \tag{31}$$

The physical indentation and deflection are obtained by multiplying the dimensionless quantities with the physical constants defined in Eqs (24), (25) and (29). The resulting force is finally obtained from Eq. (17).

7. Model for large mass impact response

During large mass impacts the plate essentially deforms as under static loading and the impactor plate system may be described as in Fig. 7b [38]. For impactor masses larger than twice the plate mass the equivalent dynamic mass of the plate may be neglected. The applied load F and midplane deflection w_p are related through:

$$F = k_{bs} w_p + k_m w_p^3 \qquad \text{where } 1/k_{bs} = 1/k_b + 1/k_s \tag{32}$$

where k_b, k_s and k_m are the bending, shear and membrane stiffnesses of the plate. For a power law load-indentation relation, Eq. (17), the indentation work is given by:

$$W_\alpha = \int F d\alpha = \int k_\alpha \alpha^q d\alpha = k_\alpha \alpha^{q+1}/(q+1) = F^{(1+1/q)} \Big/ \left[(q+1) k_\alpha^{1/q}\right] \tag{33}$$

and thus, the total deformation work W for the system is given by

$$W = \tfrac{1}{2} k_{bs} w_p^2 + \tfrac{1}{4} k_m w_p^4 + \left(k_{bs} w_p + k_m w_p^3\right)^{(1+1/q)} \Big/ \left[(q+1) k_\alpha{}^{1/q}\right] \tag{34}$$

For central impact on rectangular (quasi-) isotropic plates with side length $2A$ in the x-direction and $2B$ in the y-direction the bending stiffness may be approximated by

$$\begin{aligned} k_b &= 138\left(1 + 0.29/\overline{A}^5\right) D/(2B)^2 && \text{for clamped plates} \\ k_b &= 59\left(1 + 0.48/\overline{A}^4\right) D/(2B)^2 && \text{for simply - supported plates} \\ &\text{where } \quad \overline{A} = A/B \geq 1 \end{aligned} \tag{35}$$

which match the exact solutions [39] within 2 %. The bending stiffness for central impact on simply supported orthotropic plates may be found from Navier's solution:

$$k_b = \frac{\overline{A}\pi^4}{4(2B)^2} \Bigg/ \sum_{m=1}^{\infty} \sum_{n=1}^{\infty} \left\{ 1 \Big/ \left[D_{11} \left(m/\overline{A}\right)^4 + 2(D_{12} + 2D_{66}) m^2 n^2 / \overline{A}^2 + D_{22} n^4 \right] \right\} \tag{36}$$

m,n odd

For $\overline{A}$ >3 the stiffness is close to the asymptotic value [40] for long plates ($\overline{A}$ >>1):

$$k_b = 59 \sqrt{D^* D_{22} \sqrt{(\eta+1)/2}} \Big/ (2B)^2 \tag{37}$$

where D^* and η have been defined in Eq. (1). The bending stiffness for orthotropic plates with at least two opposite edges simply supported may be found by use of Levy's solution. For other cases the stiffness may be found by use of energy methods or by FE-analysis. A point load on a sandwich plate results, in contrast to monolithic plates, in a finite shear deflection [26]. The shear stiffness of a simply supported rectangular plate under a central point load may be approximated by the following expression:

$$k_s = S^* 1.467\left(1 + \overline{A}/10.12\right) \tag{38}$$

which matches the exact solution for isotropic thin faces [26] within 2 % for $\overline{A} \geq 1$. Note that the shear stiffness is increasing with panel aspect ratio. To the author's knowledge no closed form solutions are available for large deflections of sandwich panels under central load. Membrane effects in plates are highly dependent of the deflection shape, which is influenced by shear deformations. For circular sandwich panels with negligible shear deformation the membrane stiffness equals that of monolithic plates, which for zero core stiffness is given by

$$k_m = \overline{c}_m \pi E_{rf} 2h_f / B^2 \tag{39}$$

where $\overline{c}_m$ is a dimensionless constant, E_{rf} and h_f is the Young's modulus and thickness of the face sheets and B is the plate radius. For circular plates under central load $\overline{c}_m$ is given by [38]:

$$\begin{aligned}
&\text{CM:} \quad \overline{c}_{m1} = 191/648 \\
&\text{CI:} \quad \overline{c}_{m2} = \left[353 - 191\nu_r\right]/\left[648(1-\nu_r)\right] \\
&\text{SM:} \quad \overline{c}_{m3} = \left[\tfrac{191}{648}\chi^4 + \tfrac{41}{27}\chi^3 + \tfrac{32}{9}\chi^2 + \tfrac{40}{9}\chi + \tfrac{8}{3}\right]/\omega^4 \\
&\text{SI:} \quad \overline{c}_{m4} = \overline{c}_{m3} + \left[\tfrac{1}{4}\chi^4 + 2\chi^3 + 8\chi^2 + 16\chi + 16\right]/\left[(1-\nu_r)\omega^4\right] \\
&\text{where} \quad \chi = (1+\nu_r) \quad \omega = (3+\nu_r) \\
&\text{and} \quad \text{C = clamped, S = simply supported, M = moveable, I = imovable}
\end{aligned} \tag{40}$$

Here the membrane stiffness of a rectangular plate is approximated with an equivalent circular plate with modulus $E_{rf} = E_{rf}^*$ and equal area, i.e. with an effective plate radius

$$B^* = 2\sqrt{AB/\pi} \tag{41}$$

The peak deflection at a given energy, may be found from Eq. (34). The corresponding peak load is then found from Eq. (32). When membrane

effects are neglected (k_m=0) and the contact load is linear (q=1) the load and back face deflection resulting from an impact energy E_k are given by:

$$\begin{aligned} F &= F_{\max}\sin\left(\pi\, t/t_{imp}\right) && \text{where } F_{\max} = V_0\sqrt{Mk_\Sigma} = \sqrt{2E_k k_\Sigma} \\ w &= w_{\max}\sin\left(\pi\, t/t_{imp}\right) && \text{where } w_{\max} = F_{\max}/k_{bs} < \sqrt{2E_k/k_\Sigma} \\ t_{imp} &= \pi\sqrt{M/k_\Sigma} && \text{and} \quad t \le t_{imp}/2 \end{aligned} \tag{42}$$

where the total stiffness k_Σ is a function of indentation, bending and shear stiffness:

$$1/k_\Sigma = 1/k_\alpha + 1/k_b + 1/k_s \tag{43}$$

Prior to damage formation the total impact time will be equal to t_{imp}. This will, however, not be true after damage formation, since the load-indentation curve during loading with damage formation differs from the subsequent unloading curve.

8. Numerical examples

8.1 Prediction of indentation

In this section predictions are compared with indentation experiments on sandwich panels with the back faces supported by a rigid foundation. As a first example we consider honeycomb core sandwich panels indented by a 15 mm radius steel hemisphere [5]. The face sheets of these panels were made from Hexcel HTA/6376C carbon/epoxy tape prepreg, with the lay-ups $(0/90/\pm45)_{ns}$, n=1, 2 or 3. The cured ply data of the face sheet material are:

$E_{11}=137\,\text{GPa}$ $E_{22}=E_{33}=10.4\,\text{GPa}$ $\nu_{12}=\nu_{13}=0.31$ $\nu_{23}=0.50$
$G_{23}=4.00\,\text{GPa}$ $G_{12}=G_{13}=5.25\,\text{GPa}$ $t_{ply}=0.130\,\text{mm}$ $\varepsilon_f=0.14\,\%$

Two 5052 aluminum honeycombs with 0.001" and 0.003" foil thickness and one 48 kg/m^3 Nomex honeycomb were studied. These 1/8" cell diameter cores had the following properties:

	E_3 [MPa]	p_U [MPa]	p_{cr} [MPa]	h_c [mm]
Nomex	194	3.22	1.12	30
72 kg/m^3 Al.	1180	3.98	1.90	60
192 kg/m^3 Al.	2335	16.90	7.00	40

$\nu_{13}=\nu_{23}\approx 0$ for all three cores

The face sheets were assumed to develop delaminations with an area equivalent to circular delaminations in 30 % of the interfaces, each propagating at G_{IIc}=600 J/m^2 [30]. Figures 8 and 9 compare predictions with measurements for different combinations of cores and faces [5].

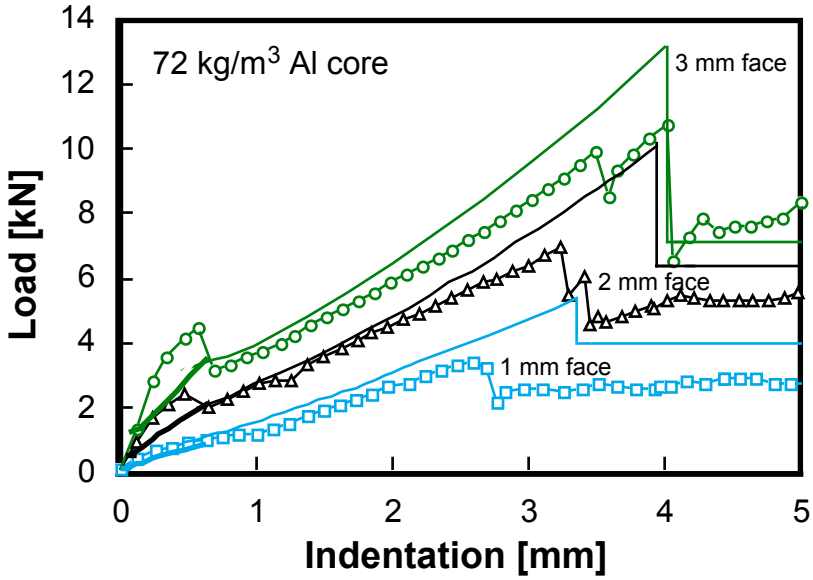

Fig. 8: Indentation of panels with core of light aluminum honeycomb
(symbols = experiments, thick/thin lines = prediction before/after delamination)

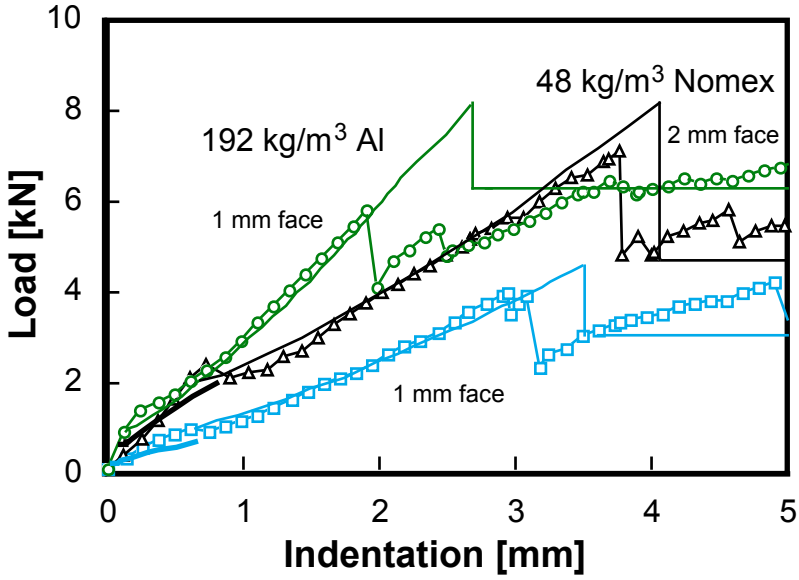

Fig. 9: Indentation of panels with cores of Nomex and heavy aluminum honeycomb
(symbols = experiments, thick/thin lines = prediction before/after delamination)

Core crushing was predicted to occur below 1 kN for all panels. The delamination threshold load and load-indentation behavior prior to fiber fracture are accurately predicted, while the predictions of fiber fracture and subsequent behavior are fairly crude. Figure 10 compares the crush radius predicted from Eq. (11) with measured damage at three different face sheet thicknesses for one of the aluminum cores [9].

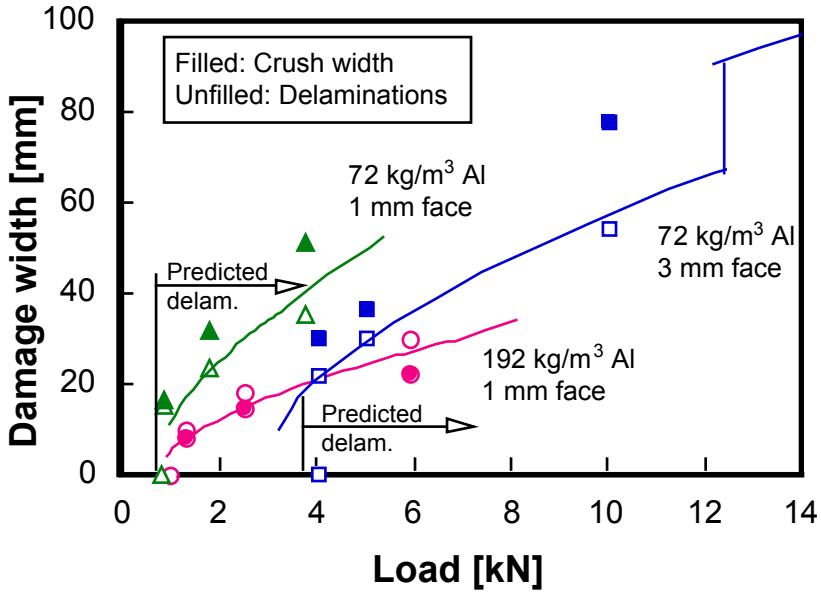

Fig. 10: Predicted and observed damage in panels with aluminum honeycomb cores. (symbols = experiments, lines = prediction

As a second example we consider foam core sandwich panels indented by 12.5, 25 and 50 mm radius steel hemispheres. The face sheets were made of two plies of glass/polyester rovimats, each consisting of a 0/90 woven roving stitched to a mat layer. This material is fairly non-linear and the selected value of E_{11} represents an average tangent modulus up to failure, rather than the initial tangent modulus, which is 14 GPa [15]. The assumed face sheet properties are [15]:

$$E_{11} = E_{22} = 12.5\,\text{GPa} \qquad E_{33} = 8\,\text{GPa} \quad \nu_{12} = 0.25 \qquad \nu_{13} = \nu_{23} \approx 0.50$$
$$G_{13} = G_{23} \approx G_{12} = 4\,\text{GPa} \qquad h_f = 2.2\,\text{mm} \quad \varepsilon_f = 0.16\% \qquad \rho = 1630\,\text{kg/m}^3$$

The face sheet contains three material interfaces, which was assumed to result in three delaminations. The mode II interlaminar toughness was estimated to G_{IIc}= 640 J/m^2 [41]. The core consisted of 80 kg/m^3 Divinycell H80 PVC foam with the properties [15, 42]:

$$E_c = 92\,\text{MPa} \quad G_c = 32.5\,\text{MPa} \quad \nu_c = 0.41 \quad p_{cr} = 1.14\,\text{MPa} \quad h_c = 22\,mm$$

The bare compressive strength is assumed to be more representative for the crush stress than the compressive strength (p_U=1.27 MPa) of the core with face sheets. Predictions and measurements [15] for three different tup diameters are shown in Fig. 11. The indentation curve assumed in [14] has been included for comparison, although the agreement with experiments is poor.

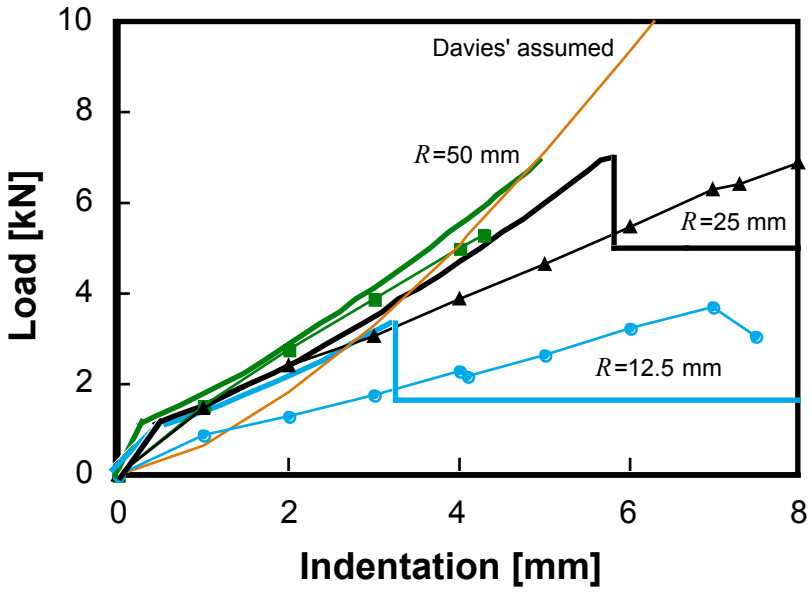

Fig. 11: Predicted and observed indentation of impacted panel (symbols = experiments, lines = prediction)

Indications of fiber fracture are noticed at 4 mm indentation for the 12.5 mm radius and at 7 mm for the 25 mm radius, in fair agreement with predictions. However, the experimental stiffness is lower and decreases more gradually than predicted, which seems to be a consequence of a skin material involving weaves and short fibers. This effect increases with decreasing tup radius, most likely as a result of premature skin cracking.

8.2 Prediction of impact response

In this section predictions are compared with impact experiments on sandwich panels with edge support, which have been selected due to the explicit measurement of back face deflection. Both panels had glass/polyester skins on a PVC foam core, with properties given in the second example of the previous section. In the impact analysis we will use a linearized indentation stiffness k_α based on Fig. 11. The resulting panel data are then as follows:

$D^* = 7140\,\text{Nm}$ $S^* = 801\,\text{kN/m}$ $E_r^* = 11.6\,\text{GPa}$ $\nu_r^* = 0.30$

$k_b = 6583\,\text{kN/m}$ $k_s = 1292\,\text{kN/m}$ $k_m = 879\,\text{MN/m}^3$ $m = 8.72\,\text{kg/m}^2$

$k_\alpha = 834\,\text{kN/m}(R = 12.5\,\text{mm})$ $k_\alpha = 1241\,\text{kN/m}(R = 50\,\text{mm})$

As a first example we consider a 800x800x25 mm sandwich panel hit at 7.67 m/s by a 2.5 kg impactor with 12.5 mm tup radius [18]. The impactor/plate mass ratio of 0.44 exceeds the limit (≤0.23) for a fully wave controlled response, but allows small mass impact response during most of the impact. Figure 12 demonstrates good agreement between predicted and observed response.

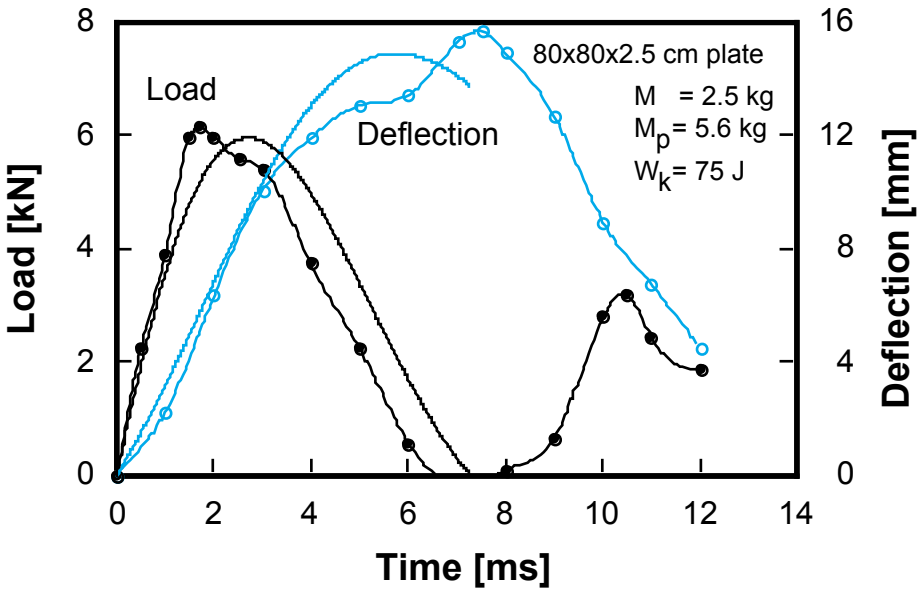

Fig. 12: Predicted and observed response for a small mass impact (symbols = experiments, lines = prediction)

As a second example we consider a 300x300x25 mm sandwich panel hit at 3.11 m/s by a 10.9 kg impactor with 50 mm tup radius [14]. The impactor/plate mass ratio of 14 guarantees an essentially quasi-static impact response. Figure 13 demonstrates a fairly good agreement between predicted and observed response. Note that the experimental deflection curve was obtained by matching a sine-function to a single peak value. Figure 14 compares predicted and observed peak load and deflection for a range of impact energies and indicates that the model not sufficiently accounts for the stiffening at larger energies. Panel stiffening occurs both due to large deflection effects and due to a growing crush area, which increases the shear stiffness. The fairly constant ratio between load and deflection indicates that the underestimated load is due to an increasing contact stiffness, which may be caused by strain rate stiffening at increasing impact velocities or by panel "wrapping" around the impactor.

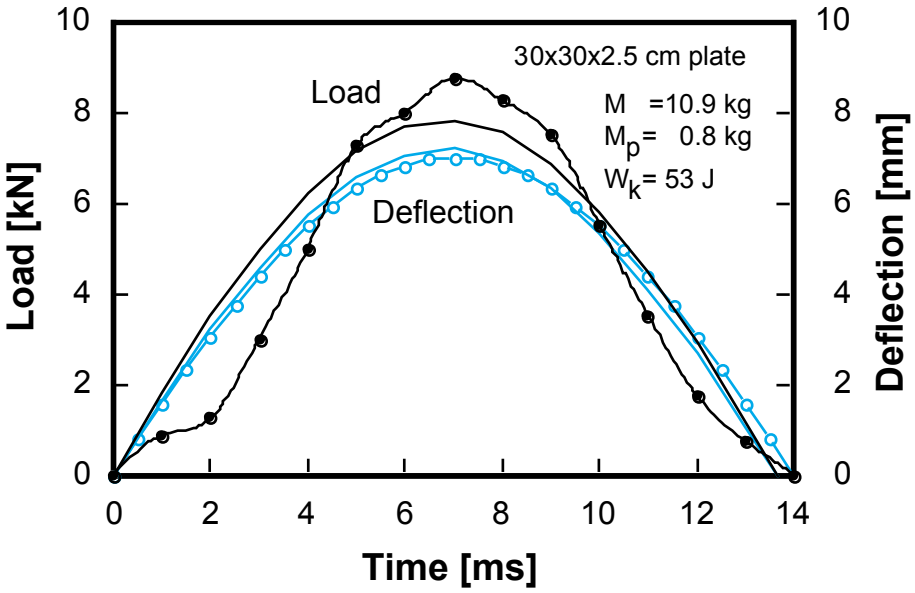

Fig. 13: Predicted and observed response for a large mass impact (symbols = experiments, lines = prediction)

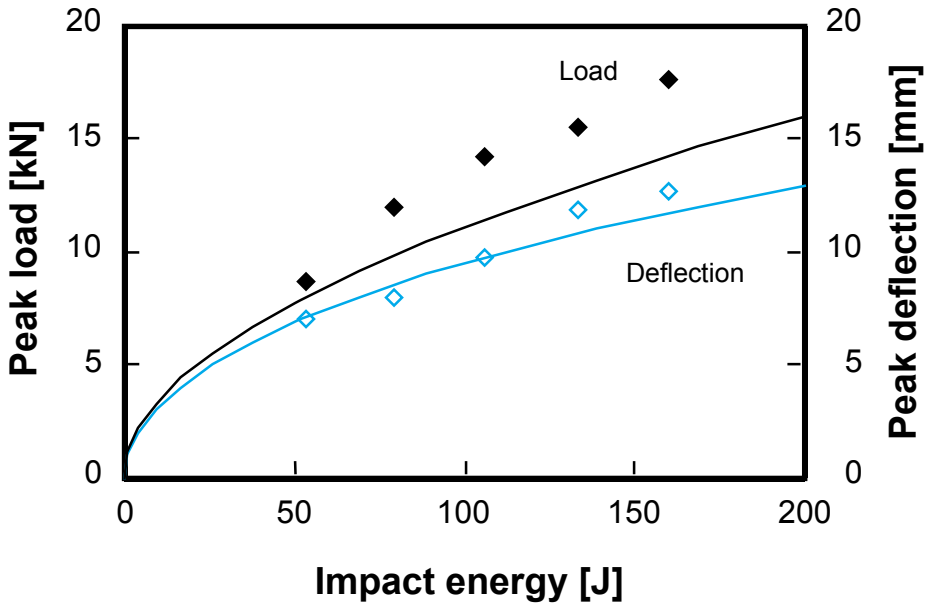

Fig. 14: Predicted and observed response for large mass impacts (symbols = experiments, lines = prediction)

9. Conclusions

An engineering method has been suggested for prediction of impact response and damage of flat sandwich panels. The approach accounts for local core crushing, delamination and large face sheet deflections and does not rely on empirical indentation laws. Different models are suggested depending on if the impactor mass is larger or significantly smaller than the mass of the impacted panel. The solution for large mass impact is based on closed form expressions which have been implemented in a spreadsheet. The solution for small mass impact may be obtained from the solution curves of a dimensionless two-parameter integral equation. The validity of the approach has been demonstrated on a number of static indentation experiments and impacts on sandwich panels. The models may replace expensive FE-simulations and are suitable for initial design of sandwich panels threatened by impact. The models are, however, limited to local indentation damage and do not allow a non-linear elastic behavior. Furthermore, the global deformation of sandwich panels is often dominated by shearing, which motivates further studies of the shear stiffness of panels with partially crushed core. From a practical point of view it is worth noting that the indentation and shear compliance may be of the same order and often dominate the impact response of sandwich panels.

Appendix A – Stiffness components

The stiffness properties of orthotropic sandwich panels may be obtained from laminated plate theory with inclusion of out-of-plane shearing [25]

$$\left(A_{ij}, B_{ij}, D_{ij}\right) = \int_{-H/2}^{+H/2} Q_{ij}\left(1, z, z^2\right) dz \quad \left(A_{44}^*, A_{55}^*\right) = \left(K_{44}A_{44}, K_{55}A_{55}\right) \tag{A1}$$

where stiffness components Q_{ij} of the core and each ply in the face sheets are considered. Effective shear stiffnesses are obtained by multiplication with shear correction factors K_{44} and K_{55}. For two identical thin stiff orthotropic face sheets on a soft core (classical sandwich theory) the core shear strain is constant (K=1) and the non-zero stiffnesses simplify to [26]:

$$\begin{aligned}
&\left[A_{11}, A_{22}, A_{12}, A_{66}\right] = \tfrac{1}{\psi}\left[E_{xf}, E_{yf}, \nu_{xyf}E_{yf}, G_{xyf}\psi\right]2h_f \\
&\left[D_{11}, D_{22}, D_{12}, D_{66}\right] = \tfrac{1}{\psi}\left[E_{xf}, E_{yf}, \nu_{xyf}E_{yf}, G_{xyf}\psi\right]h_f\left(h_c + h_f\right)^2/2 \\
&\left[A_{44}^*, A_{55}^*\right] = \left[G_{yzc}, G_{xzc}\right]\left(h_c + h_f\right)^2/h_c \\
&\text{where } \psi = 1 - \nu_{xyf}\nu_{yxf} = 1 - \nu_{xyf}^2 E_{yf}/E_{xf}
\end{aligned} \tag{A2}$$

where subscripts *f* and *c* refer to properties of the face sheet and core.

Appendix B – Derivation of delamination load

The critical load for delamination growth in the face sheet may be obtained by using the approach outlined in [31]. Within small deflection plate theory solutions may be superimposed and the deflection caused by delamination may be considered as a perturbation from the undelaminated state. Consider the deflection of a circular plate region with plate stiffness D_f and radius a_d fixed to an arbitrarily deflected outer plate region, Fig. 15.

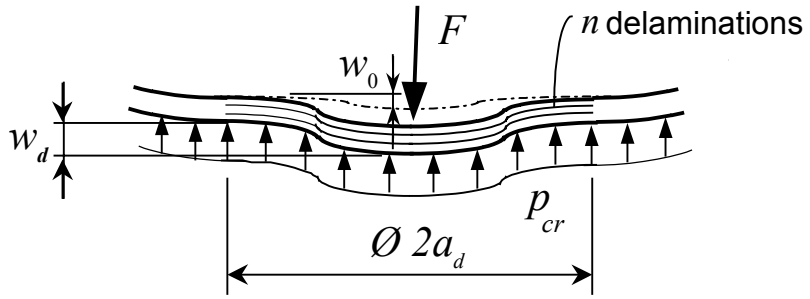

Fig. 15: Deflection of delaminated crush region

A central load F_p and a reactive pressure p_{cr} [39] causes the following deflection of the circular region

$$w_0 = \frac{F_p}{16\pi D_f}\left[a_d^2 - \tfrac{1}{4}\, p_{cr}\pi a_d^4 / F_p\right] \tag{B1}$$

n delaminations reduce the bending stiffness to $D_f/(n+1)^2$ and the resulting deflection becomes

$$w_d = (n+1)^2 w_0 = \left(n^2 + 2n + 1\right)w_0 \tag{B2}$$

Thus the delamination causes a deflection w_d - w_0 with the corresponding strain energy U_d:

$$U_d = \tfrac{1}{2}F_p\left(w_d - w_0\right) = \tfrac{1}{2}n(n+2)F_p w_0 = \frac{n(n+2)F_p^2}{32\pi D_f}\left[a_d^2 - \tfrac{1}{4}\, p_{cr}\pi a_d^4 / F_p\right] \tag{B3}$$

The strain energy release rate for a growing delaminated area is obtained from:

$$G = \frac{\partial U_d}{\partial A} = \frac{1}{2n\pi a_d}\frac{\partial U_d}{\partial a_d} = \frac{(n+2)F_p^2}{32\pi^2 D_f}\left[1 - \tfrac{1}{2}\, p_{cr}\pi a_d^2 / F_p\right] =$$

$$= \frac{(n+2)F_p^2}{32\pi^2 D_f}\left(1 - \bar{a}_d^2/2\right) \qquad \text{(B4)}$$

where $\bar{a}_d$ is defined as in Eq. (11). Delamination growth occurs in pure Mode II since all delaminated members deflect equally. Thus, the load at growth of n delaminations F_d is:

$$F_d = \pi\sqrt{32\, D_f G_{IIc} / \left[(n+2)\left(1 - \bar{a}_d^2/2\right)\right]} \qquad \text{(B5)}$$

Evidently, in sandwich panels the delamination growth load increases indefinitely with the delamination radius, while it remains constant in monolithic plates [30-31]. The delamination growth load decreases indefinitely for an increasing number of delaminations. In practice the shear stresses are non-uniformly distributed through the thickness and the first delamination occurs in the most critical (mid-plane) interface [30]. Thus, the threshold load F_{dth} for delamination initiation is obtained for an infinitesimal ($\bar{a}_d$=0) single (n=1) delamination:

$$F_{dth} = \pi\sqrt{32\, D_f G_{IIc} / 3} \qquad \text{(B6)}$$

The delamination radius a_d at an applied load F_d is obtained by combining Eqs (B5) and (B6):

$$a_d = \sqrt{F_d \bar{a}_d^2 / (\pi\, p_{cr})} \quad \text{where} \quad \bar{a}_d^2 = 2\left[1 - (F_{dth}/F_d)^2\, 3/(n+2)\right] \qquad \text{(B7)}$$

Thus, within small deflection theory the delamination radius may exceed the crush radius, since $\bar{a}_d^2 \le 2$ while $\bar{a}_p^2 \le 1.3$. When large deflections are accounted for the delamination radius should not exceed the membrane crush radius, i.e. $\bar{a}_d^2 \le \bar{a}_m^2 \le 0.7$, which corresponds to a case where membrane forces carry the entire load on the edge of the crushed region.

Appendix C – Derivation of membrane strains

Consider the axisymmetric problem of a membrane indented by a hemisphere, Fig. 5. With the origin placed in the center of the contact surface the coordinates *Z, r* are defined by:

$$(R-Z)^2 + r^2 = R^2 \quad \Rightarrow \quad Z = R\left(1-\sqrt{1-(r/R)^2}\right) \tag{C1}$$

Under the assumption that $(r/R)^{\prime} << 1$ the co-ordinate Z is given by

$$Z = \tfrac{1}{2} r^2 / R \tag{C2}$$

Outside the contact radius the shape of the membrane is assumed to be given by [22]:

$$w = \left[1 + Cs - (1+C)s^2\right] w_m \qquad \text{where} \quad s = r/a_m \tag{C3}$$

and the expression for w_m is given in [22]. The radius of contact r_1 is obtained by equating the slopes of the membrane and hemisphere. Combination of Eqs (C2) and (C3) then gives:

$$s_1 = r_1/a_m = -C \Big/ \left[a_m^2/(w_m R) - 2(1+C)\right] \tag{C4}$$

Combination of Eqs (C2) to (C4) gives the following expression for the central deflection:

$$\alpha_{Fm} = \alpha_{cr} + w(s_1) + Z(s_1) = \left[1 + Cs_1 - (1+C)s_1^2\right] w_m + \tfrac{1}{2} s_1^2 \, a_m^2 / R \tag{C5}$$

where $\alpha_{cr} = \alpha_F(F_{cr})$ is the deflection at the edge of the crushed region. The membrane stress at the membrane contact radius is obtained from equilibrium, which for small slopes gives:

$$\sigma_0 = \frac{F - p_{cr}\pi r_1^2}{2\pi h r_1 (dZ/dr)_{r=r_1}} = \frac{F\left(1 - s_1^2 \bar{a}_m^2\right) R}{2\pi h s_1^2 a_m^2} = \frac{p_{cr} R}{2h}\left(\frac{1}{s_1^2 \bar{a}_m^2} - 1\right) \tag{C6}$$

The deformation of a membrane to a spherical cap results in a uniform stress state, $\sigma_r = \sigma_\theta = \sigma_0$. Assuming plane stress ($\sigma_z \approx 0$) the strain in the cap is given by:

$$\varepsilon_0 = (1-\nu)\sigma_0 = \tfrac{1}{2}(1-\nu)\left[1 \Big/ \left(s_1^2 \bar{a}_m^2\right) - 1\right] p_{cr} R/h \tag{C7}$$

Acknowledgements

This research was funded by The Swedish Defence Materiel Administration. The complementary information on the impact experiments provided by Dr. Peter Davies at IFREMER and the suggestions by Sören Nilsson at FFA for improving the manuscript are greatly appreciated.

References

1. Abrate S. 1991. "Impact on laminated composite materials," *Appl. Mech. Rev.*, 44:155-189.

2. Abrate S. *Impact on composite structures*. Cambridge: Cambridge Univ. Press, 1998.

3. Abrate S. 1997. "Localized impact on sandwich structures with laminated facings," *Appl. Mech. Rev.,* 50:69-82.

4. Olsson, R. 1998. "Methodology for predicting the residual strength of impacted sandwich panels," *FFA TN 1997–09*, Bromma: The Aeron. Res. Inst. of Sweden.

5. Nilsson, S. 1999. "Residual compressive strength of indented sandwich panels," *FFA TN 1999-27*, Bromma: The Aeron. Res. Inst. of Sweden.

6. McGowan, D. M. and Ambur, D. R. 1998. "Damage characteristics and residual strength of composite sandwich panels impacted with and without a compression loading," *AIAA 98-1783-CP*, 39th AIAA/ASME/ASCE/AHS/ASC SDM-Conference, 1:713-723.

7. Lie, S. C., 1989. "*Damage resistance and damage tolerance of thin composite facesheet honeycomb panels*," S.M. Thesis, Dept. of Aero. and Astro., MIT, Cambridge, MA.

8. Williamson, J. E. and Lagace. P. A. 1993. "Response mechanisms in the impact of graphite/epoxy honeycomb sandwich panels," *Proc. Am. Soc. for Composites*, 8th Technical Conf., Cleveland, OH, 287–297.

9. Rinaird, O. 1995. "*Examination of indentation damage in sandwich panels*," *FFA TN 1995–36*, Bromma: The Aeron. Res. Inst. of Sweden.

10. Tsang, P. H. W. 1989. "*Impact resistance of graphite/epoxy sandwich panels*," S.M. Thesis, Dept. of Aero. and Astro., MIT, Cambridge, MA.

11. Mines, R. A. W., Worrall, C. M. and Gibson, A. G. 1990. "The response of GRP sandwich panels to dropped object impact loading," *FRC'90 Fibre Reinforced Composites*, Fourth Int. Conf., Proc. Inst. Mech. Engineers, Liverpool, 149–155.

12. Sun, C. T. and Wu, C. L. 1991. "Low velocity impact of composite sandwich panels," *AIAA paper 91-1077-CP,* AIAA 32nd Structures, Struct. Dyn. and Matls. Conf., Baltimore, MD, 1123–1129.

13. Lee, L. J., Huang. K. Y. and Fann, Y. J. 1993. "Dynamic responses of composite sandwich plate impacted by a rigid ball*," J. Compos. Mater*., 27:1238–1256.

14. Davies, P. et al. 1995. "Response of composite sandwich panels to impact loading," *Revue de l'Institut Français du Pétrole*, 50:75-82.

15. Abdul Wahab, M. A., 1997. "Etude du compertement dynamique de panneaux sandwichs a l'impact," *PhD Thesis 97.02*, Ecole Nationale Superieure d'Arts et Metiers, Bordeaux.

16. Ambur, D. R. and Cruz, J. 1995. "Low-speed impact response characteristics of composite sandwich panels," *AIAA 95-1460-CP*, 36th AIAA/ASME/ASCE/AHS/ASC SDM-Conference, 4:2681-2689.

17. Nemes, J. A. and Simmonds, K. E. 1992. "Low-velocity impact response of foam-core sandwich composites," *J. Compos. Mater.*, 26:500–519.

18. Davies, P. et al. 1995. "Impact behaviour of composite sandwich panels to impact loading," *Impact and Dynamic Fracture of Polymers and Composites*, ESIS 19, London: Mech. Engng. Publ., 341-358.

19. Horrigan, D. P. W., Aitken, R. R. and Moltschaniwskyj, G. 2000. "Modelling of crushing due to impact in honeycomb sandwiches," *J. Sandwich Struct. and Mater.*, 2:131-151.

20. Koller M. G. 1986. "Elastic impact of spheres on sandwich plates," *J. Appl. Math. Phys. (ZAMP)*, 37:256-269.

21. Olsson, R. 1998, "Theory for small mass impact on sandwich panels," *Mechanics of sandwich structures*, Proc. EUROMECH 360, Dordrecht: Kluwer, 231-238.

22. Olsson, R. and McManus, H. L. 1996. "Improved theory for contact indentation of sandwich panels," *AIAA J.,* 34:1238-1244.

23. Türk, M. H. and Hoo Fatt, M. S. 1999. "Localized damage response of composite sandwich plates," *Composites Part B*, 30:157-165.

24. Palazotto, A. N., Herup E. J. and Gummadi, L. N. B. 2000. "Finite element analysis of low-velocity impact on composite sandwich plates," *Compos. Struct.,* 49:209-227.

25. Whitney, J. M. 1987. *Structural analysis of laminated anisotropic plates,* Lancaster, PA: Technomic.

26. Zenkert, D. 1995. *An introduction to sandwich construction,* London: EMAS Ltd.

27. Olsson, R. 1994. "*Simplified theory for contact indentation of sandwich panels*," SM Thesis, Aero. and Astro. Dept., MIT (also *FFA TN 1994-33,* FFA, Sweden).

28. Vesic, A. S. 1973. *Proc. 8th Int. Conf. on Soil Mechanics and Foundation Engineering*, Moscow, 4.2:51-52.

29. Selvadurai, A. P. S. 1979. *Elastic analysis of soil-foundation interaction*, Amsterdam: Elsevier.

30. Olsson, R. 2000. "Analytical prediction of large mass impact damage in composite laminates", *FFAP H-1423*, FFA, Bromma, to appear in *Composites Part A*.

31. Robinson, P. and Davies, G. A. O. 1992. "Impactor mass and specimen geometry effects in low velocity impact of laminated composites," *Int. J. Impact Engng.*, 12:189-207.

32. Olsson, R. 2000. "Mass criterion for wave controlled impact response of composite plates", *Composites Part A*, 31:879-887.

33. Frischbier J. 1987. "Theorie der Stossbelastung orthotroper Platten und ihre experimentelle Überprüfung," *Mitteilung 51*, Bochum: Inst. für Mechanik, Ruhr-Univ.

34. Olsson, R. 1992. "Impact response of orthotropic composite laminates predicted from a one-parameter differential equation," *AIAA J.*, 30:1587-1596.

35. Mittal R K. 1987. "A simplified analysis of the effect of transverse shear on the response of elastic plates to impact loading," *Int. J. Solids Struct.*, 23:1191-1203.

36. Sneddon, I. N. 1945. “The symmetrical vibrations of a thin elastic plate,” *Proc. Camb. Philos. Soc*., 41:27–43.

37. Timoshenko, S. P. 1913. “Zur Frage nach den Wirkung eines Stoßes auf eninen Balken,” *Zeitschrift für Mathematik und Physik*, 62:198-209.

38. Shivakumar, K. N, Elber, W. and Illg W. 1985. “Prediction of impact force and duration due to low velocity impact on circular composite laminates,” *Trans. ASME, J. Appl. Mech*., 52:674–680.

39. Timoshenko, S. P, and Woinowsky-Krieger, S. 1959. *Theory of plates and shells*, New York: McGraw-Hill.

40. Lekhnitskii, S.G. 1968. *Anisotropic plates*, New York, Gordon and Breach.

41. Davies, P. 1996, "Fracture of marine composites," *Key Engng. Mater*., 121-122:583-96.

42. Davies, P. Choqueuse, D. and Pichon, A. 1994. "Influence of the foam core on composite sandwich static & impact response," *Composites Testing and Standardization*, ECCM-CTS 2, Hamburg, 513-522.